Spring 5-14-2012

Defect-Driven Dynamic Model of Electrostatic Discharge and Endurance Time Measurements of Polymeric Spacecraft Materials

Charles Sim
Utah State University

Alec Sim
Utah State University & Irving Valley College

JR Dennison
Utah State University

Matthew Stromo
Utah State University and College of the Desert

Defect-Driven Dynamic Model of Electrostatic Discharge and Endurance Time Measurements of Polymeric Spacecraft Materials

USU Materials Physics Group

Charles Sim, Alec M. Sim, JR Dennison, and Matthew Stromo

Utah State University, Logan, Utah 84322-4415

Phone: (859) 559-3302, FAX: (435) 797-2492, E-mail: charles.the.sim@gmail.com

UtahStateUniversity MATERIALS PHYSICS GROUP

12th Spacecraft Charging Technology Conference 14-18 May, 2012 Kitakyushu, Japan

Experimental Chamber

Figure 1

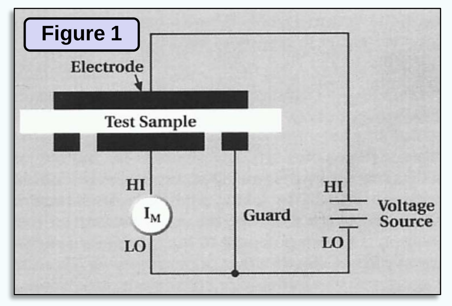

Figure 2

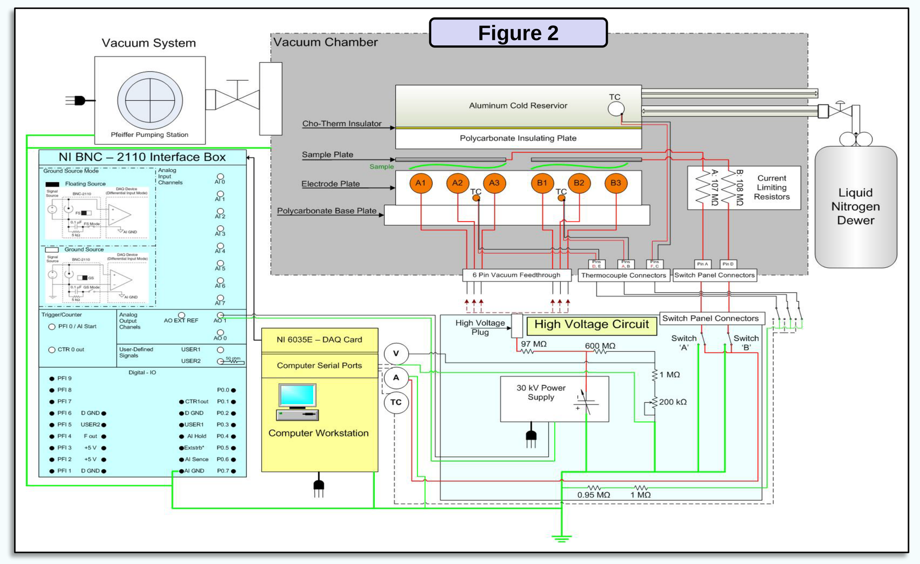

Fig. 1. Simple parallel plate capacitor assembly for the ESD test circuit.

Fig. 2. Electrostatic Discharge Chamber test circuit detailed schematic.

Tests were conducted in a custom, high vacuum chamber in a simple parallel plate capacitor assembly designed by the Utah State University Materials Physics Group, shown in Fig. 1. A more detailed schematic of the system is shown in Fig. 2.

Samples were clamped between a metal sample mounting plate and six Cu or graphite foam covered high voltage electrodes (Figs. 3 and 4). Voltage was applied to the electrode using a variable high voltage power. The voltage was incremented at a rate of 21 V every 4 s, until the target voltage was reached or breakdown had occurred. Current and voltage are monitored using two interfaced multimeters under LabVIEW control. Two 100 MΩ resistors are used to the limit the current in the circuit after complete breakdown occurs.

Measurements for the time endurance of electrostatic breakdown (see Fig. 10) were conducted by ramping the applied voltage to a target plateau voltage and maintaining this static electric field until breakdown occurred. Endurance time to breakdown, t_{en}, was measured from the moment an electric field was applied.

Target voltages for the endurance time experiments were in the range of 4000 V to 9000 V. These values yield endurance times from a few seconds to a few days.

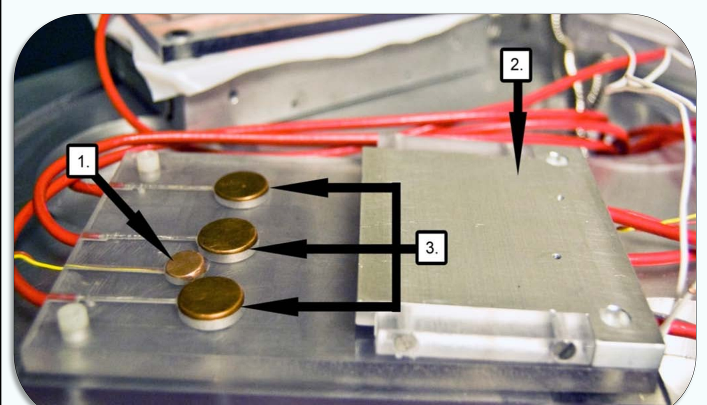

Fig. 6. Exposed view of ESD sample assembly. (1) Cu thermocouple mount, (2) Sample and mounting plate, (3) Cu high voltage electrodes.

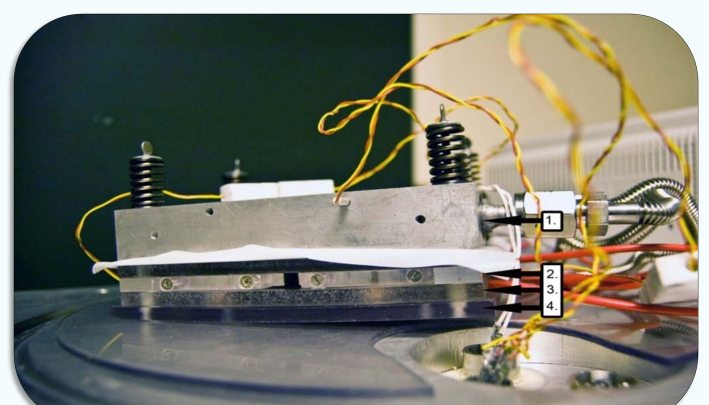

Fig. 7. Interior view of ESD sample assembly. (1) Cryogen reservoir, (2) Sample mounting plate, (3) Electrode plate with 2 sets of 3 high voltage copper electrodes and a Cu thermocouple mount, (4) Polycarbonate insulating base.

Acknowledgements

Research was supported by funding from the NASA/JWST Electrical Systems Working Group at Goddard Space Flight Center, a USU URCO grant, and the Utah State University Physics Department Howard L. Blood Memorial Scholarship.

References

[1] R.D Leach and M.B. Alexander, "Failures and anomalies attributed to spacecraft charging," NASA Reference Publication 1375, NASA Marshall Space Flight Center, August 1995.
[2] C.L. Griffiths, J. Freestone, R.N. Hampton, "Thermoelectric Aging of Cable Grade XLPE," Conf. Record of IEEE International Symposium on Electrical Insulation, Arlington, VA, 1998, pp. 578-582.
[3] C. Dang, J.-L. Parpal, J.P. Crine, "Electrical Aging of Extruded Dielectric Cables: Review of Existing Theory and Data," IEEE Trans. Dielectrics and Insulators, Vol. 3, No. 2, April 1996, 237-247.
[4] Lewis, T.J., Llewellyn, J.P., van der Sluijs, M.J., Freestone, J. and Hampton, R.N., 1996, Seventh International Conference on Dielectric Materials Measurement and Applications, 23-26 September, IEE Conference Publication Number 430, pp220 – 224.
[5] A. Sim, "Unified Model of Charge Dynamics in Highly Insulating Materials," Ph.D. Dissertation, Dept. Physics, Utah State University, Logan, UT, 2011.
[6] Charles Sim, Alec Sim, Douglas Ball and JR Dennison, "Temperature and Endurance Time of Electrostatic Field Strengths of Polymeric Spacecraft Insulators," 11*th Spacecraft Charging Technology Conference*, (Albuquerque, NM, September 20-24, 2010).
[7] M. L. Wald, "Giving the Grid Some Backbone," Sc. Am. Earth 3D, 19(1), 52-57 (2009).
[8] D. Hastings, H. Garrett, Spacecraft-Environment Interactions, New York, NY: Cambridge Press, 1996.
[9] K. Shinyama, S. Fujita; Int. J. Soc. Mater. Eng. Resour. 13, 2 (Mar 2006)].
[10] Anthony Thomas, JR Dennison, Steve Hart and RC Hoffmann, "The Effect of Voltage Ramp Rate on Dielectric Breakdown of Thin Film Polymers,' American Physical Society Four Corner Section Meeting, Utah State University, Logan, UT, October 6-7, 2006.

Abstract

Measurements of the electrostatic field strength of thin film insulating materials due to interactions with the space plasma environment are one of the most important concepts to understand for the effective design of spacecraft. It is therefore critical to understand how electrostatic field strength (F_{ESD}) of spacecraft materials varies due to environmental conditions such as temperature, duration of applied electric field, rate of field changes, and history of exposure to high fields. This research STUDY emphasizes experimental and theoretical investigations on the FESD of polymeric insulators as a function of temperature, applied field, and time to breakdown. It suggests that values of F_{ESD} from standard handbooks or cursory measurements that have been used routinely in the past by the spacecraft charging community substantially overestimate the field required for breakdown in common spacecraft situations.

Electrostatic discharge tests for two prototypical materials with different types of trap state densities—low density polyethylene (LDPE) and polyimide (PI or Kapton HN™)—were conducted by applying a high voltage across the material in parallel plate geometry using a modified ASTM D149-99 method. F_{ESD} was determined as a sustained, rapid rise in I-V curves measured in a custom, high vacuum chamber (<10^{-3} Pa base pressure) over a temperature range of ~120 K to ~320 K. Time dependent breakdown was found by applying a static voltage across the material and measuring the endurance time (the time before electrostatic breakdown occurs under an applied electric field stress). Endurance times were measured from 10^0 s to 10^5 s at voltages >50% below the nominal breakdown voltage. Ramp rate dependence was found by varying the rate and magnitude of the incremental voltage step used to reach electrostatic breakdown. Slower ramp rates (as low as 20 V steps at 4 s intervals) resulted in substantially lower F_{ESD} values than tests conducted the maximum ramp rate of 500 V/s recommended in ASTM 3755 standards. Very short, unsustained arcing was also observed beyond a material dependant threshold electric field; the frequency of these arcs was field dependant. For LDPE, a small linear temperature dependence of F_{ESD} for LDPE was observed in the range of 150 K to 240 K. Above 240 K there was a shift in F_{ESD} near a structural phase transition in LDPE, at which other electrostatic properties have also exhibited discontinuities.

These experimental results are compared with thermodynamic mean field multiple trapping models of the electric field induced aging process and available measurements. Numerous studies have shown that electrical aging can be characterized by defect creation within the material from bond stress due to local and applied electric fields. We introduce a modified dynamic temperature-dependent electrostatic discharge model which accurately predicts observations of two distinct regions of negative logarithmic decay of the endurance time as a function of applied field, which are attributed to separate recoverable and irrecoverable defect mechanisms. Relevant examples of both recoverable and irrecoverable defect mechanisms are discussed; these are characterized by two parameters, a mean separation of sites and an activation energy. The interdependence of these mechanisms may explain the unusual transition observed in the crossover field region between the mechanisms. The observed frequency of the short unsustained arcs is consistent with the recoverable defect part of the model. We further discuss these results in terms of a more comprehensive unified theory for electron transport in highly disordered insulating materials, which allows a correlation between fitting parameters and more fundamental materials properties such as atomic scale structure and bonding, mobility, transition probabilities, and spatial and energetic distributions of trap states.

Electrostatic Breakdown Theory

Electrical aging causes breakdown in insulating materials. Aging in the spacecraft environment is induced by high energy particle flux into or though the material, medium to high applied fields, and contact carrier injection. It has been shown by many authors that electrical aging can be characterized by the Gibbs free energy for bond destruction, trap creation within the material, and bond stress due to local and applied fields.

Assuming that an applied field produces a pressure on a defect, we find that the pressure is related to the permittivity times the square of the field (1). The defect energy is simply the pressure times the effective volume over which the field acts. In most cases, the effective volume is proportional to the inverse of the density of states (10^{18}-10^{20}) cm^{-3}. The average cohesive bond energy associated with (weak Van der Waals bonds and main chain reconfiguration energies such as chain kinks) can be estimated as (2-10 meV) and using (1) one can estimate the minimum field at which recoverable defects might begin to occur, called the critical field F_{onset} ~ 4 MeV/m. Such energies are low enough that thermal fluctuations can lead to defect annihilation. Further, we can estimate complete bond breaking energy as (0.6 eV - 0.9 eV) giving F_{bb}~270 MeV/m.

$$E_{defect} = \frac{1}{2}(F_c)^2(\epsilon_0\epsilon_r\Delta V) \quad (1)$$

And this yields the critical onset and bond breaking fields

$$F_{onset} = \sqrt{\frac{E_{recoverable}}{(\epsilon_0\epsilon_r\Delta V)}} \qquad F_{bb} = \sqrt{\frac{E_{irrecoverable}}{(\epsilon_0\epsilon_r\Delta V)}}$$

This model, based on rate theory and the idea that the bond breaking kinetics should be similar to kinetic rate reactions in chemical systems, provides a way to calculate the increase in trap concentration, (broken bonds) as a function of time and temperature (3). Stress acts on the bond energies (Gibbs energy of activation *ΔG*) to reduce the energy necessary to start the degradation process (Fig 12). For simple average molecular interactions, a process can be envisioned where the field increases or decreases the Gibbs energy. On average it is expected that the forward and backward movements of on-chain carriers, chain reconfiguration and free chain elements can be thought of as a rate process (2). The rate of bond breaking due to the field, Gibbs activation energy ΔG, activation volume ΔV, temperature *T*, and applied field *F* are the physical parameters of the system. Using (2-3) one can obtain (4).

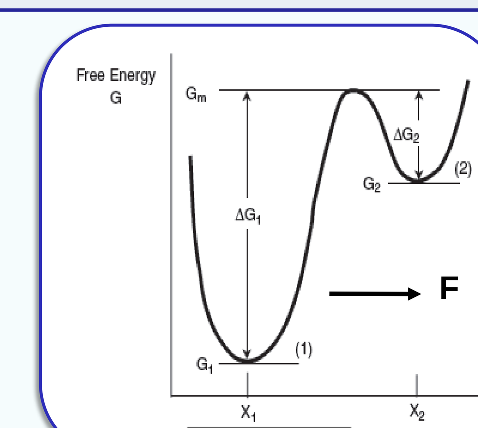

Figure 12

The measured endurance time data in Figure 11 shows that there is a definite transition between two separate regimes, suggesting that a new composite model incorporating at least two mechanisms is required. Consider two breakdown processes a and b in Fig. 10. In process a, the breakdown of the material is due to creation of new traps resulting from charge injection and impact ionization of molecular or crystalline segments. This process requires less energy to initiate (activation energy), allows for spontaneous repair of broken bonds, and is dominant at fields below the bond breaking field, where the ends of broken bonds with unpaired sites will act as electron traps. As the injected charge becomes trapped in the ionized molecular segments and on chain segments, a high localized field develops leading to breakdown. In process b, the breakdown of the material is due to direct stress on molecular segments causing irreparable damage with no bond repair possible. In this process there, is little ionization or segmental motion.

$$K^{\pm}{}_{bb} = \frac{kT}{h} exp\left[-\frac{\Delta G_{bb} \pm \epsilon\Delta V_{bb}F^2}{2kT}\right] \quad (2)$$

$$\frac{dn_{bb}(t)}{dt} = K_{bb}[F,T,n_{bb}(t)](N_t - n_{bb}(t)) + K_{br}[F,T,n_{bb}(t)]n_{bb}(t) \quad (3)$$

$$t_{end}(F,T) = \left(\frac{h\,P(F,T)}{2k_bT}\right)\exp\left[\frac{\Delta G(F,T)}{k_bT}\right]\mathrm{csch}\left[\frac{F^2\varepsilon_0\varepsilon_r\Delta V_{def}(F,T)}{2k_bT}\right] \quad (4)$$

t_{end} is the time to breakdown. The activation energy, *ΔG*; the number density of defects, n_{def} ; and probability function, *P* are the fitting parameters of the model. Planck's constant *h*, the Boltzmann distribution constant k_b, and the permittivity constant ε_0 are fundamental physical constants. The value of ε_r is the relative dielectric constant and a property of the material. The applied field F and temperature T are variables that can be changed with each test. A dual mechanism model has been developed that provides a way to calculate the increase in trap concentration (rate of bond breaking) as a function of time and applied stress [5]. The probability of breakdown during a time Δt while the sample is held at field F is the sum of breakdown for each of the mechanisms:
(5).

$$P(F,T) = \sum_{\substack{i=dual\\ mechanisms}}\left(\frac{2k_bT}{h/\Delta t}\right)\exp\left[\frac{-\Delta G_i(F,T)}{k_bT}\right]\sinh\left[\frac{F^2\varepsilon_0\varepsilon_r\Delta V_i(F,T)}{2k_bT}\right] \quad (5)$$

Analysis of Breakdown Results

Pre-Breakdown Analysis

In the pre-breakdown region, the material being tested has very his resistance and negligible (<10 μA) current flows. Several spikes in the current (green highlighted regions of Figs. 5, 6 and 11) can be seen before breakdown. These are the short duration, recoverable breakdown events that occur only after the critical field value, F_{onset}, has been reached, beyond which eventual breakdown is only a matter of time.

A statistical analysis has been conducted on the many "current spikes" observed for 65 breakdown I-V runs. This analysis yields critical information about the nature of ESD, arcing, and the distinction between recoverable and irrecoverable breakdown.

The frequency of pre-breakdown arcs is shown in Fig. 8. The estimated amplitude of a single arc is 0.2±0.1 μA. At higher electric fields, measured arc currents are larger, suggesting that multiple arcs-typically of ~1 μs duration—have occurred during the ~0.5 s data acquisition times of the multimeters. The frequency of arcs is fit with an exponentially increasing function (see Fig. 9) with amplitude N_0=3.1 Hz and onset energy F_{onset}=53 MV/m.

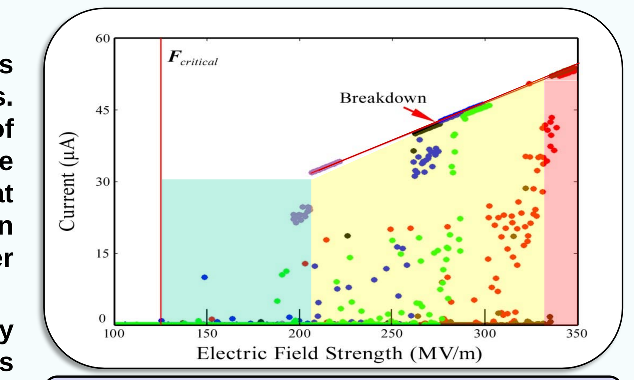

Figure 5. Six I-V curves of current as a function of applied voltage, where voltage is ramped at 21 V increments at 4 sec intervals until breakdown.

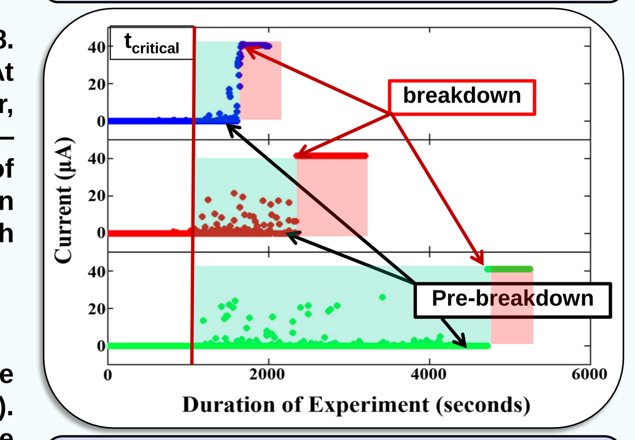

Figure 6. Three endurance curves of current as a function of time, where the applied voltage is ramped up to a set value and then maintained until complete breakdown occurs.

Breakdown Analysis

At breakdown (red regions), low resistance paths are formed and the current increases significantly (≥10 μA). After breakdown, a constant slope is maintained set by the current limiting resistance in the circuit (Fig. 5).

For insulating polymer Low Density Polyethylene (LDPE) 27 μm thick samples, the mean room temperature breakdown field occurs at (277 8) MV/m and is the upper bound below which endurance time tests were conducted.

Figure 8

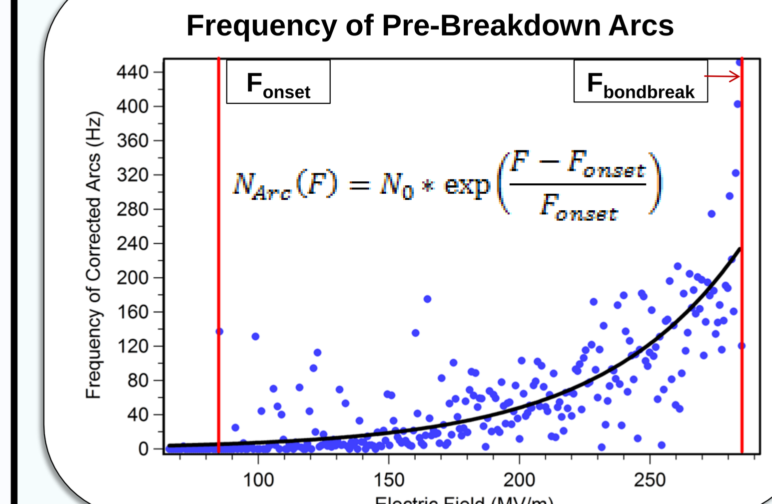

Figure 8. A statistical analysis conducted of the many observed short duration, recoverable breakdown events or "current spikes" observed during 65 breakdown I-V runs. The fitting parameters of the exponential function are N_0=3.1 Hz, F_{onset}=53 MV/m. $F_{bondbreak}$ is at 284 MV/m

Figure 9

$$N_{Arc}(F) = N_0 * \exp\left(\frac{F - F_{onset}}{F_{onset}}\right)$$

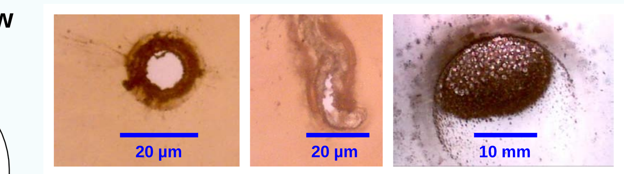

Fig. 7. Images of breakdowns. Kapton E usually breaks down with circular holes (left), while LDPE is more irregular (center). ePTFE can breakdown rather spectacularly (right).

Figure 10

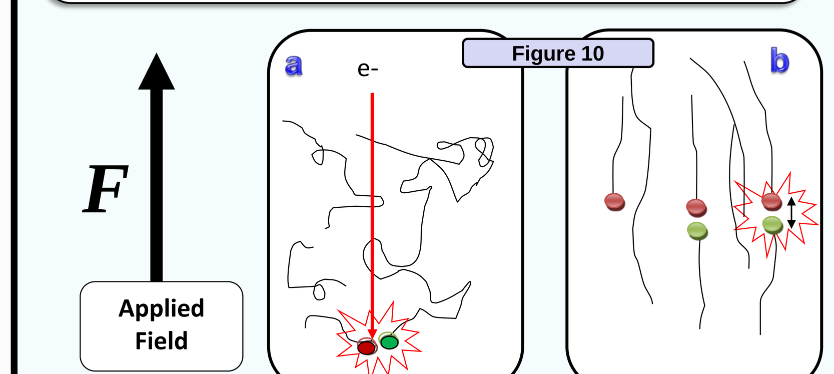

Figure 11

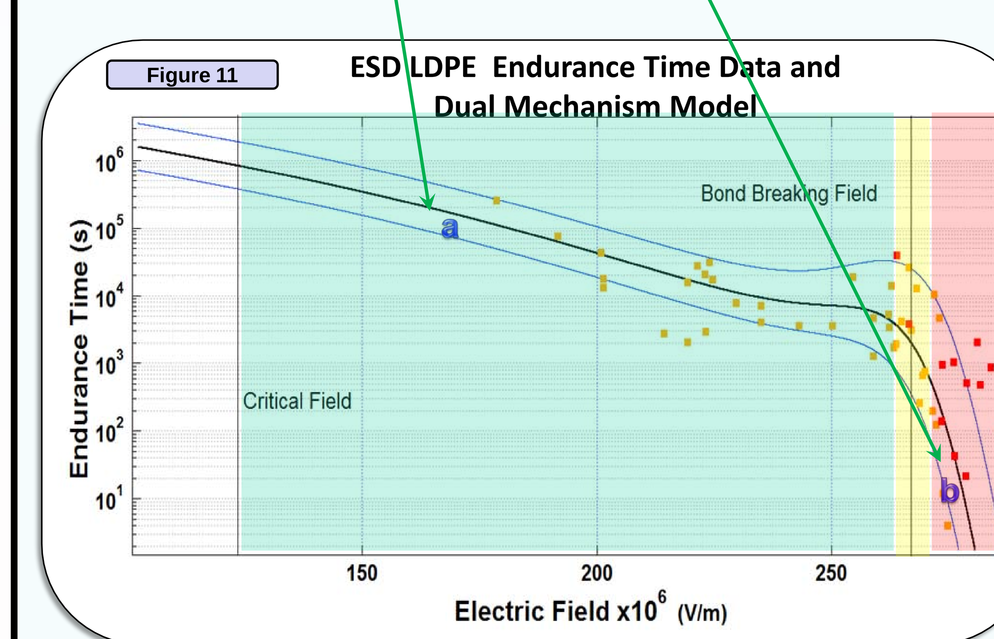

Endurance Time Analysis

Tests on the endurance time to breakdown in the material LDPE were conducted at electric fields in the range of 172 to 280 MV/m.

Breakdown tests conducted in the range of 172 to 255 MV/m were dominated by the recoverable pre-breakdown process (Figs. 10a and 11a). Breakdown times observed in this range were on the order of a few hours to several days.

Tests conducted in the 265 to 284 MV/m range were dominated by the irrecoverable breakdown process. Breakdown times observed here were on the order of a few minutes to ~1 hr.

Tests conducted in the 260±5 MV/m range demonstrate a transition region, in which the irrecoverable breakdown process is beginning to dominate over the recoverable breakdown process as the electric field is increased. Breakdown times observed here are on the order of 1 to 10 hours.

Based on fits to the data using Eq. 5, the measured values for the Gibbs activation energy and activation volume are ΔG_{Pre} = 0.90 eV and ΔG_{BD} = 3.50 eV; ΔV_{Pre} ~ 10^{-20} cm^3 and ΔV_{BD} ~ 10^{-19} cm^3 [6].

Figure 10. Breakdown processes a and b. Process a, recoverable breakdowns: Breakdown of the material is due to creation of new traps resulting from charge injection and impact ionization of molecular or crystalline segments. Process b, irrecoverable breakdowns (F > $F_{bondbbreak}$): Breakdown of the material is due to direct stress on molecular segments causing irreparable damage with no bond repair possible.

Figure 11. Dual mechanism multiple trapping model fit against endurance time data for the polymer LDPE. In addition, note the blue min and max lines. These are obtained by assuming a 2% deviation in ΔG and ΔV. This set of curves clearly gives an encompassing prediction of the possible spacecraft destruction times for applied fields. In fact, the most important line on this graph is the minimum blue line which gives the fastest possible time to breakdown. This is the important design curve.

(a) Breakdown process dominated by the reconfiguration and de-cohesion of molecular bonds acted upon by charge injection. (b) Breakdown process dominated by direct stress of the electric field acting on the molecular bonds causing permanent damage. The colored lines to the right indicate the following time scales on the graph: 1 minute, 1 hour, 1 day, 1 week.